CHINESE OPTICS LETTERS

Vol. 20, No. 11 | November 2022

Visible light communication system at 3.59 Gbit/s based on *c*-plane green micro-LED

Guoqiang Li (李国强)[1,†], Runze Lin (林润泽)[1,†], Haichao Guo (郭海超)[2,3], Pengfei Tian (田朋飞)[1*], and Nan Chi (迟 楠)[1**]

[1] Department of Communication Science and Engineering, Institute for Electric Light Sources, Key Laboratory for Information Science of Electromagnetic Waves (MoE), School of Information Science and Technology, Fudan University, Shanghai 200433, China

[2] National Key Laboratory of Science and Technology on Space Microwave, Xi'an 710100, China

[3] China Academy of Space Technology (Xi'an), Xi'an 710100, China

*Corresponding author: pftian@fudan.edu.cn

**Corresponding author: nanchi@fudan.edu.cn

Received April 18, 2022 | Accepted June 10, 2022 | Posted Online July 14, 2022

Visible light communication (VLC) based on the micro light emitting diode (micro-LED) has attracted increasing attention owing to its high bandwidth, low power consumption, and high security. Compared with semi-polar or non-polar micro-LEDs, the commercial polar micro-LED has the advantages of low cost and more mature epitaxy technique. In this study, green micro-LEDs with different indium tin oxide (ITO) sizes are fabricated based on the commercial *c*-plane LED epitaxial wafer. The transmission performance of 80, 100, and 150 μm devices has been studied in detail. A partial pre-equalization scheme is utilized to increase data rates. Finally, the VLC system with a 100 μm green micro-LED as the transmitter could achieve a maximum data rate of 3.59 Gbit/s. Such a result will be beneficial to promote the further development of low-cost, high-speed VLC devices in the future.

Keywords: micro-LED; visible light communication; *c*-plane; discrete multi-tone.

DOI: 10.3788/COL202220.110602

1. Introduction

Visible light communication (VLC), as a new type of communication technology, has the characteristics of no electromagnetic radiation, being license-free, and high security compared with traditional radio frequency (RF) communication[1–3]. It is expected to become an important supplement to the current wireless communication technology. In order to achieve a high-speed VLC system, the high-performance optical transmitter (Tx) is one of the most critical factors. Compared with the traditional light emitting diode (LED) device, GaN-based micro-LEDs can further realize the advantages of high bandwidth and low power consumption due to its micron-level size[4]. Therefore, the micro-LED has been widely used in the fields of micro-display, free-space optical (FSO) communication, underwater wireless optical communication (UWOC), and so on[5–7]. Especially for VLC application, the single-chip modulation bandwidth of up to 1.5 GHz and a data rate of 11.74 Gbit/s can be achieved by the non-polar blue micro-LED and series-biased blue micro-LED, respectively[8,9].

Compared with the widely reported blue micro-LED, the "green gap" problem caused by the high In composition of multiple quantum wells (MQWs) has always hindered the realization of high-performance GaN-based green micro-LEDs[10]. In recent years, semi-polar or non-polar green micro-LEDs have been gradually investigated, which are expected to avoid the drawbacks caused by conventional epitaxy growth on the *c*-plane substrate[11,12]. Data rates beyond 5 Gbit/s have been achieved by parallel arrays of semi-polar green micro-LEDs[13]. However, although current researches reveal the potential of semi-polar or non-polar green devices in high-speed VLC, the shortcomings such as complex epitaxy technique and high cost have not been resolved yet. Therefore, if the high-performance VLC system can be realized by commercial polar green micro-LEDs, the results will also be undoubtedly valuable for the low-cost and high-speed VLC systems due to the more mature epitaxy technique.

In this work, we measured the performance of green micro-LEDs with different sizes based on the commercial *c*-plane LED epitaxial wafer in detail and analyzed the VLC performance of such devices at different working conditions by combining the bit loading discrete multi-tone (DMT) modulation format and digital pre-equalization technology. Finally, a 100 μm micro-LED was used to achieve a maximum data rate of 3.59 Gbit/s. The realization of such a high-performance VLC system does not require a complex epitaxial structure design. It is expected that such devices can have broad application prospects in different fields such as Internet of Things and smart lighting.

2. Performance of Micro-LEDs

Figure 1 shows the structure of the green micro-LED, which includes a sapphire substrate, a buffer layer, an n-type GaN layer, a MQW layer, a p-type GaN layer, and a limited current spreading layer (indium tin oxide, ITO). The fabrication process has been reported in detail in our previous work[14]. The overall size of the single pixel is 300 μm × 300 μm. However, different from the fabrication of traditional micro-LEDs, by limiting the area of the ITO layer instead of the dry etching process, the current of green micro-LEDs in our work can also be limited to a specific area to achieve high current density, which will ensure the small-scale emission area. What is more, the performance degradation caused by sidewall defects introduced by the etching process can be minimized. In addition to being a solid-state source for lighting and display, such micro-LEDs also have the potential for photodetection applications[14]. It can be seen from Fig. 1 that unlike the limited current injection area when used as a Tx, when the device is used as a photodetector, the InGaN/GaN MQW as an optical absorption layer has a total area of 300 μm × 300 μm, which can achieve high-sensitivity detection for incident optical signals. Especially for VLC application, this feature will improve the signal-to-noise ratio (SNR) at the receiver (Rx), thereby ensuring the communication performance of the whole system. Such a monolithic integrated multifunctional micro-LED will help realize miniaturized high-performance duplex VLC technology.

Figures 2(a) and 2(b) are the current-voltage (*I-V*) curves and the light output power-current (*P-I*) curves of micro-LEDs with different sizes (80, 100, and 150 μm, referring to the sizes of ITO layers), respectively. In order to prevent irreversible damage due to the excessively high operating current, the maximum current was limited to the value where the light output power of the device was saturated. It can be seen that as the sizes increase, the maximum operating current and light output power also increase simultaneously, which are 100, 160, 210 mA and 0.848, 1.365, 2.120 mW, respectively. The corresponding maximum current densities are 1562.5, 1600, 933.3 A/cm^2. Although 80 μm and 100 μm micro-LEDs are confined by the electrical injection areas and their maximum light output powers are less than that of the 150 μm device, they can also achieve much higher injection current densities, which are important for improving the electrical-to-optical modulation bandwidths of such micro-LEDs.

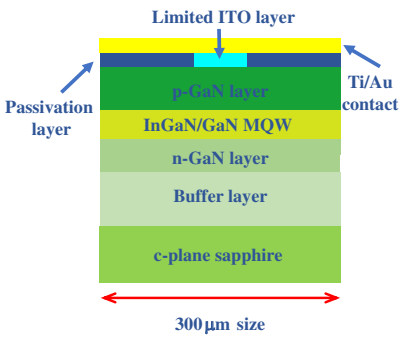

Fig. 1. Schematic structure of multi-functional green micro-LED.

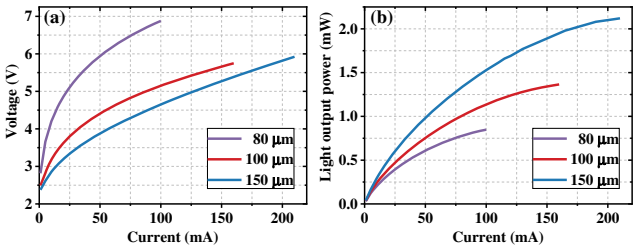

Fig. 2. (a) *I-V* curves and (b) *P-I* curves of multi-functional green micro-LEDs with different sizes.

In order to further explain the influence of current density on the modulation bandwidth, the frequency response curves of a 100 μm device at different current densities are shown in Fig. 3(a). As the current density ranges from 100 A/cm^2 to 1500 A/cm^2, the −3 dB bandwidth of the device increases significantly (from 41.6 MHz to 139 MHz). This is mainly due to the decrease in the differential carrier lifetime caused by the increased carrier density. Figure 3(b) shows the current density versus modulation bandwidth curves of 80, 100, and 150 μm devices, respectively. At the same current density, even if the device sizes are different, the corresponding modulation bandwidths are still basically same. However, due to the difference in effective injection area, the maximum current density of a large-size device is much lower than that of a small-size device, which will affect the maximum available bandwidth and limit the performance of the VLC system. The maximum electrical-to-optical modulation bandwidths of 80, 100, and 150 μm devices are 131.20 MHz (1562.5 A/cm^2), 147.33 MHz (1600 A/cm^2), and 97.1 MHz (933.3 A/cm^2), respectively.

The electroluminescence (EL) spectra have also been tested in detail. Figure 4(a) represents the EL spectra of the 100 μm device at different currents. Figures 4(b) and 4(c) are the peak wavelength and full width at half-maximum (FWHM) curves extracted from the spectra as a function of current density. It can be seen that for the 100 μm micro-LED, the peak wavelength first changes from 523.1 nm (1 mA) to 513.6 nm (90 mA) and then gradually increases to 515.4 nm (160 mA). The blue shift is mainly due to the band filling effect and the suppression of the quantum-confined Stark effect (QCSE) as the carrier density

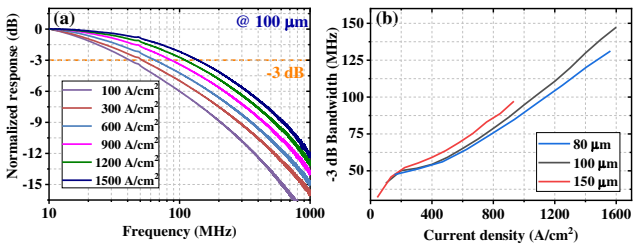

Fig. 3. (a) Frequency response curves of the 100 μm micro-LED at different current densities. (b) Modulation bandwidth versus current density curves of 80, 100, and 150 μm devices, respectively.

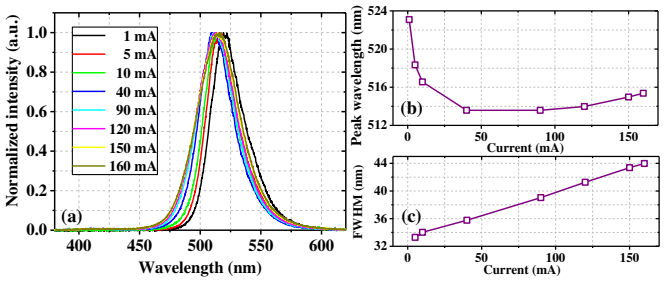

Fig. 4. EL spectra characteristics of 100 μm micro-LED. (a) Spectra at different currents. (b) Peak wavelength and (c) FWHM versus current curves.

increases[15]. The red shift can be attributed to the self-heating effect of the micro-LED at high operating current[16].

In addition to the change of the peak wavelength, the phenomenon of spectrum broadening will also appear. When the current is 5 mA, the FWHM of the 100 μm device is 33.3 nm. For the maximum current (160 mA), the FWHM of the device is broadened to 44.0 nm, an increase of 32.1%. The most obvious impact of spectral change is the problem of color shift, which is particularly critical in the display application. For the multifunctional device that integrates lighting, display, duplex VLC, and other functions, how to reduce the spectrum shift will be studied in our future research.

3. Experimental Setup and Results

The experimental setup and photograph of the micro-LED-based VLC system are shown in Fig. 5. The bit loading DMT modulation format was utilized to raise spectral efficiency, and it achieved a high data rate. Herein, 122 subcarriers were modulated with DMT modulation. Firstly, the channel estimation was done offline by sending a quadrature phase shift keying (QPSK) training sequence. The channel frequency response obtained from the channel estimation was used for further pre-equalization. The SNR among different DMT subcarriers for bit loading modulation was obtained by calculating the error

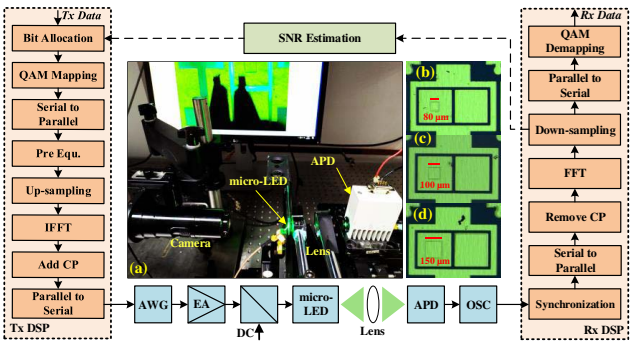

Fig. 5. Experimental setup of the micro-LED-based VLC system. (a) Photograph of the optical system showing the micro-LED, lens group, and APD. Micrographs of three different sizes of micro-LEDs: (b) 80 μm; (c) 100 μm; (d) 150 μm.

vector magnitude (EVM) of QPSK symbols[17]. Based on the specific SNR table, the quadrature amplitude modulation (QAM) order of bit allocation for different subcarriers was determined. The SNR table corresponding to different modulation levels is calculated at a target bit error rate (BER) of 3.8×10^{-3}. Then, after QAM mapping and DMT modulation, the bit loading DMT signal was generated and sent to an arbitrary waveform generator (AWG, Tektronix, AWG710B).

To overcome the bandwidth limitation of the micro-LED, digital pre-equalization was utilized before DMT modulation at the Tx. Based on zero-forcing equalization[18], the transmitted signal was pre-emphasized as

$$X'(f) = X(f)H(f)^{-\alpha}, \tag{1}$$

where $X(f)$ was the original transmitted signal, $H(f)^{-\alpha}$ represented the inverse of channel frequency response, and α was a scaling factor of the pre-equalization. When $\alpha = 1$, the pre-equalization fully compensated the channel response to flatten the received spectrum, which was called full pre-equalization. However, full pre-equalization resulted in the decrease of the overall SNR when compensating for the high-frequency components of the signal, thus degrading the system performance[19]. It had been demonstrated that partial pre-equalization can address this contradictory trade-off and achieve a better system performance[20]. In the experiment, we changed the scaling factor α to adjust the ratio of partial pre-equalization. Specifically, we set α as 0.5 and compare its performance with that of full pre-equalization.

The signal output from the AWG was amplified by an electrical amplifier (EA, Mini-Circuits, ZHL-2-8-S+) and DC-biased with a bias-tee (Mini-Circuits, ZFBT-6GW+). Then, via a high-speed probe, the biased signal was fed into the green micro-LED to finish electro-optical conversion. Micrographs of three different sizes of micro-LEDs are represented in Figs. 5(b)–5(d). In this paper, the transmission performances of these micro-LEDs will be discussed.

By applying a lens group, the optical signal from the micro-LED was collimated and focused on the avalanche photon diode module (APD, Hamamatsu, C5658). The APD was employed to finish photoelectric conversion. The output signal of the APD was captured by the oscilloscope (Agilent DSA-X 96204Q). In offline digital signal processing (DSP), the signal was first synchronized and then sent to DMT demodulation. After DMT demodulation, the QAM symbol was used to calculate the BER.

The achievable data rates and light output powers are determined by the operating points of the LEDs[21]. Without pre-equalization, we search for the optimal operating points at a signal bandwidth of 750 MHz to better compare the transmission performances of three types of micro-LEDs. Figure 6 describes the measured data rates for different driven current and signal peak-to-peak voltage (V_{pp}). At a fixed signal V_{pp} of 0.8 V, the data rates of three types of micro-LEDs increase firstly and then decrease with the increase of the driven current, as shown in Fig. 6(a). It can be seen that the micro-LED with a larger size may achieve a maximum data rate at a greater driven

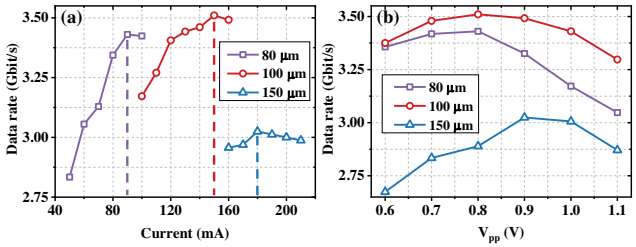

Fig. 6. Measured data rates for (a) different driven current with V_{pp} = 0.8 V, (b) different signal V_{pp} with optimal bias current (90 mA, 150 mA, and 180 mA for 80, 100, and 150 μm devices, respectively).

current. The optimal driven currents for 80, 100, and 150 μm are 90, 150, and 180 mA, respectively. The transmission performance of the 100 μm micro-LED is better than that of the 80 μm micro-LED due to the higher SNR from the higher light output power. However, limited by the modulation bandwidth, the 150 μm device achieves the lowest data rate though it has the highest light output power. There is a tradeoff between the modulation bandwidth and the SNR. It is expected that the 150 μm device may achieve a higher data rate in a long distance between the Tx and Rx when the SNR is the dominant factor. At the selected driven current, the optimal signal V_{pp} of the micro-LEDs is also found, as shown in Fig. 6(b). Similar trend of data rates can be seen in Fig. 6(b). With a small V_{pp}, the signal is in low SNR conditions. However, a too-large V_{pp} induces signal clipping, which results in nonlinear impairments. These two situations decrease the achievable data rates. The optimum values of signal V_{pp} are 0.8 V for the 80 and 100 μm devices and 0.9 V for the 150 μm device. The 100 μm device has the best transmission performance among the three types of micro-LEDs.

Then, pre-equalization performance is tested using the 100 μm micro-LED as the Tx. The corresponding results are represented in Fig. 7. Pre-equalization widens the effective modulation bandwidth at the cost of the SNR loss. There is a tradeoff between the widened modulation bandwidth and SNR loss. Experimental results show that full pre-equalization over-compensates the frequency response, thus severely degrading the SNR, resulting in the decreasing of the data rate. Partial

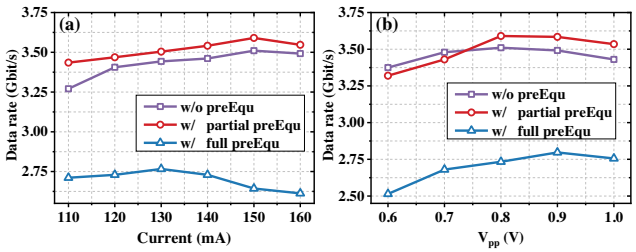

Fig. 7. Measured data rates of 100 μm micro-LED without pre-equalization, with partial or full equalization for (a) different driven current and (b) different signal V_{pp}.

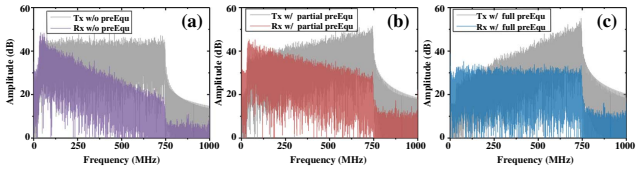

Fig. 8. Frequency spectrum comparison of transmitted signal and received signal: (a) without pre-equalization; (b) with partial pre-equalization; (c) with full pre-equalization.

pre-equalization helps to raise the transmission data rate and performs better with a larger signal V_{pp}, where the modulation bandwidth is the dominant factor. However, when the VLC system is in SNR limitation (with a low signal V_{pp}), partial pre-equalization will also bring performance loss for the system because pre-equalization improves the system performance at the expense of SNR. The results with partial and no equalization are very similar. Bit loading is an effective modulation method, which takes the channel condition into consideration. Herein, we use pre-equalization to further enhance the performance of the system. Compared with full pre-equalization, partial pre-equalization holds a balance between spectrum compensation and the SNR loss, and thus it achieves a higher data rate.

To better understand the performance of full and partial pre-equalization, we measure the frequency spectra of the transmitted signal and received signal, as shown in Fig. 8. Without pre-equalization, the received spectrum will continuously decrease as the signal bandwidth increases. Hence, the signal at the high-frequency region is severely attenuated. A higher data rate can be achieved by spectrum compensation. With full pre-equalization, the low-frequency region of the transmitted spectrum is greatly attenuated, and the high-frequency region is enhanced according to the inverse of the channel frequency response. As a result, the received spectrum is relatively flat under the whole signal bandwidth, but the amplitude of the spectrum is very low, which means that the allocated SNR for each DMT subcarrier is not enough to realize high-order modulation. As a comparison, partial pre-equalization holds a balance between spectrum compensation and the SNR loss, thus achieving the best system performance.

Employing partial pre-equalization, the data rates for different signal bandwidths of three types of micro-LEDs are measured at optimum current and V_{pp}. The corresponding results are represented in Fig. 9(a). The maximum data rates of 80 μm

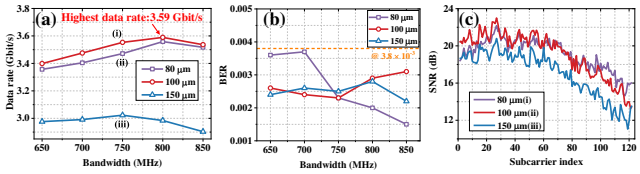

Fig. 9. (a) Measured data rates and (b) BERs for different signal bandwidths. (c) SNR versus subcarrier index at the signal bandwidth of 750 MHz.

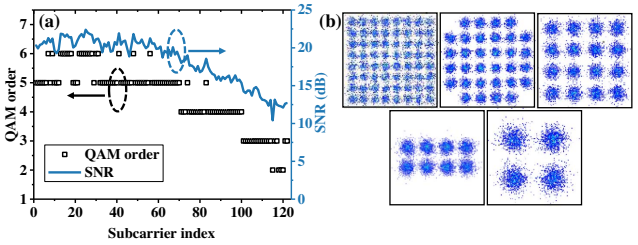

Fig. 10. (a) QAM order and SNR versus subcarrier index of 100 μm micro-LEDs at the highest data rate. (b) Corresponding constellation diagrams.

and 100 μm micro-LEDs are achieved with the signal bandwidth of 800 MHz, and that of 150 μm is obtained with 750 MHz bandwidth. The 100 μm micro-LED obtains the highest data rate of 3.59 Gbit/s. The highest data rates of the 80 μm and 150 μm devices are 3.58 Gbit/s and 3.02 Gbit/s, respectively. It should be noted that the data rates are achieved with the BER under 7% forward error correction (FEC) threshold of 3.8×10^{-3}, as Fig. 9(b) shows. Such a BER is measured with a constant power since the current and V_{pp} are determined at the optimum operating point. The SNR versus the subcarrier index at the signal bandwidth of 750 MHz is shown in Fig. 9(c). As a comparison, the lowest SNR of the 150 μm device results in poor system performance.

Figure 10(a) shows the QAM order and SNR versus subcarrier index of 100 μm micro-LEDs at the highest data rate. The QAM order follows the trend of the SNR, and the highest QAM order can be up to six at the low-frequency region. The corresponding constellation diagrams are shown in Fig. 10(b).

4. Conclusion

We designed and fabricated a new type of micro-LEDs with different sizes, which can integrate solid-state lighting (SSL), micro-display, and duplex VLC functions. By testing the optical and electrical characteristics of 80, 100, and 150 μm devices, the maximum light output powers of 0.848, 1.365, and 2.120 mW were obtained, respectively. For the micro-LED, the smaller injection area will bring higher current density, thereby effectively increasing the maximum modulation bandwidth. The maximum modulation bandwidths of the 80, 100, and 150 μm devices are 131.20 MHz (1562.5 A/cm^2), 147.33 MHz (1600 A/cm^2), and 97.1 MHz (933.3 A/cm^2), respectively. In addition, we also analyzed the potential impact of spectral changes due to the operating current. On the basis of device research, by combining bit loading DMT modulation and digital pre-equalization technology, we tested the best operating points of devices with different sizes and analyzed the impact of equalization technology. Finally, by using a 100 μm micro-LED with the best performance as the Tx, a data rate of 3.59 Gbit/s was achieved. Such a high-speed VLC system proves the communication potential of multi-functional micro-LEDs, which will play an important role in the future of ultra-high-speed duplex VLC and further integrated intelligent optoelectronic systems.

Acknowledgement

This work was supported by the National Key Research and Development Program of China (Nos. 2021YFE0105300, 2021YFB3601000, and 2021YFB3601003), National Natural Science Foundation of China (Nos. 61925104, 62171137, and 62031011), Major Key Project of PCL (No. PCL2021A14), Science and Technology Commission of Shanghai Municipality (No. 21511101303), and Leading-edge Technology Program of Jiangsu Natural Science Foundation (No. BE2021008-2).

†These authors contributed equally to this work.

References

1. N. Chi, H. Haas, M. Kavehrad, T. D. Little, and X.-L. Huang, "Visible light communications: demand factors, benefits and opportunities [Guest Editorial]," IEEE Wirel. Commun. **22**, 5 (2015).
2. L. E. M. Matheus, A. B. Vieira, L. F. Vieira, M. A. Vieira, and O. Gnawali, "Visible light communication: concepts, applications and challenges," IEEE Commun. Surv. Tutor. **21**, 3204 (2019).
3. C. Wang, G. Li, F. Hu, Y. Zhao, J. Jia, P. Zou, Q. Lu, J. Chen, Z. Li, and N. Chi, "Visible light communication for vehicle to everything beyond 1 Gb/s based on an LED car headlight and a 2 × 2 PIN array," Chin. Opt. Lett. **18**, 110602 (2020).
4. K. J. Singh, Y.-M. Huang, T. Ahmed, A.-C. Liu, S.-W. H. Chen, F.-J. Liou, T. Wu, C.-C. Lin, C.-W. Chow, and G.-R. Lin, "Micro-LED as a promising candidate for high-speed visible light communication," Appl. Sci. **10**, 7384 (2020).
5. X. Zhou, P. Tian, C.-W. Sher, J. Wu, H. Liu, R. Liu, and H.-C. Kuo, "Growth, transfer printing and colour conversion techniques towards full-colour micro-LED display," Prog. Quantum Electron. **71**, 100263 (2020).
6. E. Xie, X. He, M. S. Islim, A. A. Purwita, J. J. McKendry, E. Gu, H. Haas, and M. D. Dawson, "High-speed visible light communication based on a III-nitride series-biased micro-LED array," J. Lightwave Technol. **37**, 1180 (2018).
7. S. Zhu, X. Chen, X. Liu, G. Zhang, and P. Tian, "Recent progress in and perspectives of underwater wireless optical communication," Prog. Quantum Electron. **73**, 100274 (2020).
8. A. Rashidi, M. Monavarian, A. Aragon, A. Rishinaramangalam, and D. Feezell, "Nonpolar m-plane InGaN/GaN micro-scale light-emitting diode with 1.5 GHz modulation bandwidth," IEEE Electron Device Lett. **39**, 520 (2018).
9. E. Xie, R. Bian, X. He, M. S. Islim, C. Chen, J. J. McKendry, E. Gu, H. Haas, and M. D. Dawson, "Over 10 Gbps VLC for long-distance applications using a GaN-based series-biased micro-LED array," IEEE Photon. Technol. Lett. **32**, 499 (2020).
10. M. Usman, M. Munsif, U. Mushtaq, A.-R. Anwar, and N. Muhammad, "Green gap in GaN-based light-emitting diodes: in perspective," Crit. Rev. Solid State Mat. Sci. **46**, 450 (2021).
11. Y. Zhao, H. Fu, G. T. Wang, and S. Nakamura, "Toward ultimate efficiency: progress and prospects on planar and 3D nanostructured nonpolar and semipolar InGaN light-emitting diodes," Adv. Opt. Photonics **10**, 246 (2018).
12. Y.-H. Chang, Y.-M. Huang, W. H. Gunawan, G.-H. Chang, F.-J. Liou, C.-W. Chow, H.-C. Kuo, Y. Liu, and C.-H. Yeh, "4.343-Gbit/s green semipolar (20-21) μ-LED for high speed visible light communication," IEEE Photonics J. **13**, 7300204 (2021).
13. G.-R. Lin, H.-C. Kuo, C.-H. Cheng, Y.-C. Wu, Y.-M. Huang, F.-J. Liou, and Y.-C. Lee, "Ultrafast 2 × 2 green micro-LED array for optical wireless communication beyond 5 Gbit/s," Photonics Res. **9**, 2077 (2021).
14. G. Zhou, R. Lin, Z. Qian, X. Zhou, X. Shan, X. Cui, and P. Tian, "GaN-based micro-LEDs and detectors defined by current spreading layer: size-dependent characteristics and their multifunctional applications," J. Phys. D **54**, 335104 (2021).
15. X. Zhao, B. Tang, L. Gong, J. Bai, J. Ping, and S. Zhou, "Rational construction of staggered InGaN quantum wells for efficient yellow light-emitting diodes," Appl. Phys. Lett. **118**, 182102 (2021).

16. Z. Gong, S. Jin, Y. Chen, J. McKendry, D. Massoubre, I. M. Watson, E. Gu, and M. D. Dawson, "Size-dependent light output, spectral shift, and self-heating of 400 nm InGaN light-emitting diodes," J. Appl. Phys. **107**, 013103 (2010).
17. R. A. Shafik, M. S. Rahman, and A. R. Islam, "On the extended relationships among EVM, BER and SNR as performance metrics," in *International Conference on Electrical and Computer Engineering* (2006), p. 408.
18. C. B. Ribeiro, M. L. de Campos, and P. S. Diniz, "Zero-forcing equalization for time-varying systems with memory," in *IEEE International Symposium on Circuits and Systems* (2004), p. V413.
19. G. Li, P. Zou, F. Hu, C. Wang, G.-R. Lin, and N. Chi, "Frequency slicing pre-equalization scheme for laser diode based underwater visible light communication," in *Asia Communications and Photonics Conference* (2020), paper S4B.1.
20. Y. Zhou, J. Shi, Z. Wang, J. Zhang, X. Huang, and N. Chi, "Maximization of visible light communication capacity employing quasi-linear preequalization with peak power limitation," Math. Probl. Eng. **2016**, 6902152 (2016).
21. R. Bian, I. Tavakkolnia, and H. Haas, "15.73 Gb/s visible light communication with off-the-shelf LEDs," J. Lightwave Technol. **37**, 2418 (2019).